



Cite this: *Environ. Sci.: Processes Impacts*, 2022, **24**, 1303

## Evaluating atmospheric mercury (Hg) uptake by vegetation in a chemistry-transport model†

Aryeh Feinberg, \*<sup>a</sup> Thandolwethu Dlamini, <sup>a</sup> Martin Jiskra, <sup>b</sup> Viral Shah <sup>c</sup> and Noelle E. Selin \*<sup>ad</sup>

Mercury (Hg), a neurotoxic heavy metal, is transferred to marine and terrestrial ecosystems through atmospheric transport. Recent studies have highlighted the role of vegetation uptake as a sink for atmospheric elemental mercury ( $Hg^0$ ) and a source of Hg to soils. However, the global magnitude of the  $Hg^0$  vegetation uptake flux is highly uncertain, with estimates ranging 1000–4000 Mg per year. To constrain this sink, we compare simulations in the chemical transport model GEOS-Chem with a compiled database of litterfall, throughfall, and flux tower measurements from 93 forested sites. The prior version of GEOS-Chem predicts median  $Hg^0$  dry deposition velocities similar to litterfall measurements from Northern hemisphere temperate and boreal forests ( $\sim 0.03\text{ cm s}^{-1}$ ), yet it underestimates measurements from a flux tower study ( $0.04\text{ cm s}^{-1}$  vs.  $0.07\text{ cm s}^{-1}$ ) and Amazon litterfall ( $0.05\text{ cm s}^{-1}$  vs.  $0.17\text{ cm s}^{-1}$ ). After revising the  $Hg^0$  reactivity within the dry deposition parametrization to match flux tower and Amazon measurements, GEOS-Chem displays improved agreement with the seasonality of atmospheric  $Hg^0$  observations in the Northern midlatitudes. Additionally, the modelled bias in  $Hg^0$  concentrations in South America decreases from  $+0.21\text{ ng m}^{-3}$  to  $+0.05\text{ ng m}^{-3}$ . We calculate a global flux of  $Hg^0$  dry deposition to land of 2276 Mg per year, approximately double previous model estimates. The Amazon rainforest contributes 29% of the total  $Hg^0$  land sink, yet continued deforestation and climate change threatens the rainforest's stability and thus its role as an important Hg sink. In an illustrative worst-case scenario where the Amazon is completely converted to savannah, GEOS-Chem predicts that an additional 283 Mg Hg per year would deposit to the ocean, where it can bioaccumulate in the marine food chain. Biosphere–atmosphere interactions thus play a crucial role in global Hg cycling and should be considered in assessments of future Hg pollution.

Received 27th January 2022  
Accepted 21st April 2022

DOI: 10.1039/d2em00032f  
[rsc.li/espi](http://rsc.li/espi)

### Environmental significance

Vegetation uptake is one of largest sinks of atmospheric mercury (Hg) from the atmosphere and a major source of Hg to soils. We better quantify its importance to the global biogeochemical Hg cycle by updating an atmospheric chemistry model with information from newly available measurement datasets. Our revised dry deposition scheme yields improved model agreement with atmospheric Hg seasonality in Northern midlatitudes and Hg concentrations in South America. We calculate a dry deposition flux to land that is approximately double previous model estimates. Using our revised model, we also illustrate the potential importance of land-atmosphere feedbacks: the conversion of the Amazon rainforest to savannah leads to an additional transfer of 283 Mg Hg each year to the ocean due to a reduced land sink.

## 1. Introduction

Mercury (Hg) is a neurotoxic heavy metal that bioaccumulates in marine and terrestrial food webs as methylmercury (MeHg). Approximately 8000 Mg per year of Hg are emitted to the atmosphere each year, of which 30% are emitted directly by anthropogenic sources, 10% are from natural geogenic sources, and 60% are re-emissions of anthropogenic Hg that was previously deposited to land and water.<sup>1</sup> Atmospheric Hg is transported to remote regions due to its long lifetime of around 6 months before being ultimately removed by wet and dry deposition.<sup>2,3</sup> Recent studies have emphasized the role that vegetation plays in the dry deposition of elemental mercury ( $Hg^0$ ), with

<sup>a</sup>Institute for Data, Systems, and Society, Massachusetts Institute of Technology, Cambridge, MA, USA. E-mail: [arifein@mit.edu](mailto:arifein@mit.edu); [selin@mit.edu](mailto:selin@mit.edu)

<sup>b</sup>Environmental Geosciences, University of Basel, Basel, Switzerland

<sup>c</sup>Harvard John A. Paulson School of Engineering and Applied Sciences, Harvard University, Cambridge, MA, USA

<sup>d</sup>Department of Earth, Atmospheric, and Planetary Sciences, Massachusetts Institute of Technology, Cambridge, MA, USA

† Electronic supplementary information (ESI) available. See <https://doi.org/10.1039/d2em00032f>



estimates of this sink ranging from 1000 to 4046 Mg per year.<sup>4–6</sup> Isotopic evidence suggests that atmospheric Hg<sup>0</sup> deposition is the source of 57–94% of all Hg in soils.<sup>5</sup> Due to this link between atmospheric Hg and the biosphere, atmospheric Hg levels can be altered by seasonality and trends in vegetation productivity.<sup>4</sup> Climate change and anthropogenic activities could disturb the Hg vegetation sink through multiple processes, *e.g.*, deforestation,<sup>7</sup> CO<sub>2</sub> fertilization,<sup>8</sup> vegetation species shifts,<sup>9</sup> drought,<sup>10</sup> and ice storms.<sup>11</sup> In particular, there is a risk that the Amazon, the largest rainforest on the planet, could transition into a savannah-like ecosystem due to anthropogenic pressures (*i.e.* deforestation) and climate change.<sup>12–14</sup> An accurate representation of Hg<sup>0</sup> vegetation uptake in the global Hg budget is essential for predicting the impact of these perturbations on Hg cycling. However, until now there has been only narrow validation of atmospheric Hg chemistry models with observations of vegetation uptake, mainly focusing on selected sites in North America.<sup>9,15–17</sup>

Almost all atmospheric Hg chemistry models (including GEOS-Chem, ECHMERIT, GEM-MACH-Hg, and GLEOMS) use a resistance-based dry deposition scheme.<sup>15,18</sup> In these schemes, canopy uptake processes are parametrized as a function of leaf area index (LAI) and land cover type.<sup>19,20</sup> There is considerable uncertainty associated with the model parameters related to Hg dry deposition.<sup>5</sup> The evaluation of model parametrizations is complicated by the systematic biases inherent to different experimental methods quantifying the uptake of Hg by vegetation (Table 1). Litterfall measurements are used to determine the amount of Hg taken up by foliage over a growing season, which isotopic evidence suggests mainly originate from atmospheric Hg<sup>0</sup> uptake as opposed to oxidized mercury (Hg<sup>2+</sup>).<sup>21–23</sup>

Measurements of throughfall (water falling through the forest canopy) capture another portion of dry deposited Hg, washing off Hg adsorbed to canopy surfaces.<sup>24</sup> Isotope evidence suggests that 34% to 82% of Hg in throughfall is derived from adsorbed atmospheric Hg<sup>0</sup>.<sup>25</sup> However, litterfall and throughfall measurements do not account for uptake of Hg by woody tissues, mosses, and lichens in forest ecosystems.<sup>6,25</sup> Whole ecosystem net Hg<sup>0</sup> exchange has been measured directly by micrometeorological methods, which employ tower measurements and flux-gradient calculations.<sup>24,26</sup> Micrometeorological techniques also measure net ecosystem exchange fluxes at higher time resolutions (30 min) than throughfall and litterfall measurements. Despite being the more accurate technique, there is currently only one annual micrometeorological measurement from a temperate deciduous forest site<sup>26</sup> to compare with atmospheric model predictions.

Past studies have calculated a broad range of magnitudes for the global Hg vegetation sink, depending on the monitoring data and scaling approach used. Wang *et al.*<sup>27</sup> estimated that 1180 ± 710 Mg Hg per year deposits as litterfall, using a compilation of litterfall data and statistical modeling. Total throughfall has been estimated to contribute 1338 Mg per year over forests, which includes both wet deposition and dry-deposited Hg washed off leaves.<sup>28</sup> By extrapolating flux tower measurements from Harvard Forest, Obrist *et al.*<sup>26</sup> calculated a global Hg<sup>0</sup> uptake flux of 3162–3813 Mg per year, approximately a factor of three higher than the litterfall assessment.<sup>27</sup> A new global database approach, considering other vegetation components in addition to litterfall, also reported a larger estimate for the global vegetation uptake flux: 2705 ± 504 Mg per year.<sup>6</sup> It remains unclear how these larger fluxes can be

**Table 1** Review of measurement methods quantifying Hg vegetation uptake, compared in this study with GEOS-Chem simulated Hg<sup>0</sup> dry deposition in forested areas

| Name                                   | Description   | Species of Hg                                   | Potential biases when comparing with modelled Hg <sup>0</sup> dry deposition   |
|--|---|---|--|
| Litterfall                             | Collecting and analyzing plant litter to measure net Hg uptake in leaves over the growing season                  | Hg <sup>0</sup> <sup>a</sup>                    | Missing uptake from woody tissues, lichens, mosses, and soil; missing Hg <sup>0</sup> contribution from throughfall; foliar re-emission not explicitly modelled  |
| Throughfall                            | Measuring flux of Hg washed off leaves during precipitation events with a collector placed under the canopy       | Hg <sup>0</sup> , Hg <sup>2+</sup> <sup>b</sup> | — <sup>c</sup>   |
| Total foliar uptake                    | Calculated as litterfall + throughfall – open field wet deposition  | Hg <sup>0</sup> , Hg <sup>2+</sup>              | Missing uptake from woody tissues, lichens, mosses, and soil; includes Hg <sup>2+</sup> contribution from throughfall; foliar re-emission not explicitly modelled  |
| Micrometeorological flux tower methods | Using Hg <sup>0</sup> tower measurements and flux-gradient calculations to calculate whole net-ecosystem exchange | Hg <sup>0</sup>                                 | Only one annual measurement available in forested areas; <sup>26</sup> if soil emissions are high, net-ecosystem exchange underestimates Hg <sup>0</sup> vegetation uptake; foliar re-emission not explicitly modelled |

<sup>a</sup> Demers *et al.*,<sup>21</sup> Jiskra *et al.*,<sup>22</sup> Zheng *et al.*,<sup>23</sup> <sup>b</sup> Wang *et al.*,<sup>25</sup> <sup>c</sup> Throughfall is not directly compared to modelled Hg<sup>0</sup> dry deposition.



accommodated within the global Hg budget and whether they are compatible with other observational constraints in the Hg cycle, *e.g.*, atmospheric concentrations, wet deposition fluxes, and isotopic tracers.<sup>29</sup> Global atmospheric models like GEOS-Chem are useful tools for evaluating these broader constraints on the global Hg budget. However, recent work suggests that global atmospheric models underestimate vegetation uptake compared to tropical litterfall data<sup>5</sup> and net exchange fluxes measured over a midlatitude deciduous forest.<sup>26</sup>

In this study, we amend the Hg<sup>0</sup> dry deposition scheme in GEOS-Chem to integrate information derived from a broad dataset of available vegetation uptake measurements. We focus our comparison between model and measurements in forested sites, since forests are expected to have the largest contribution to vegetation uptake.<sup>30</sup> By adjusting the biological reactivity of Hg<sup>0</sup> in the dry deposition scheme, we propose model configurations that are compatible with different vegetation uptake measurement methods (litterfall; total foliar uptake; micrometeorological net Hg<sup>0</sup> exchange, see Table 1). We evaluate the impacts of these adjustments on the modelled atmospheric Hg seasonality and spatial distribution. Using the model configuration that best matches available observational constraints, we provide improved estimates of the global magnitude of the vegetation sink and other Hg budget terms. We explore the effect of an extreme scenario for Amazon land cover change on the fate of atmospheric Hg and discuss its implications for future Hg cycling. Finally, we discuss future directions for the development of model parametrizations of Hg vegetation uptake.

## 2. Materials and methods

### 2.1 Compilation of litterfall, throughfall, and dry deposition measurements

To evaluate the performance of the GEOS-Chem dry deposition scheme in simulating Hg<sup>0</sup> dry deposition over forests, we compiled an observational database of vegetation uptake measurements for forested areas. We focused on studies which measured litterfall, throughfall, and/or open field wet deposition. For study sites where all three quantities were measured, we calculated a total foliar uptake flux = litterfall + throughfall – open field wet deposition, which represents the total dry deposited Hg to foliage.<sup>24</sup> In addition, we evaluate the model against net ecosystem exchange flux of Hg<sup>0</sup> at a temperate deciduous hardwood forest site.<sup>26</sup>

We used previous reviews of Hg dry deposition as starting points for the database.<sup>24,31,32</sup> To identify more recent litterfall studies, we screened 334 results from a Web of Science (Clarivate Analytics) search with the term “mercury litter\*”. In total, the database contains 79 publications with measurement-based estimates of Hg uptake fluxes. We extracted additional metadata from the compiled publications: geographic coordinates, altitude, year of study, and land cover type (ESI† Spreadsheet).

The database ranges temporally from 1987 to 2020. Regional trends in atmospheric Hg<sup>0</sup> concentrations also affect the magnitude of Hg<sup>0</sup> uptake fluxes over this time period; for example, Hg<sup>0</sup> has decreased by ~1–2% per year over North

America and Europe from the 1990s to 2010s.<sup>33</sup> To compare simulations directly with Hg fluxes, it would be necessary to conduct longer term simulations or reduce the dataset to a selected time period. Instead, we compare modeled Hg<sup>0</sup> dry deposition velocities to calculated annual mean Hg<sup>0</sup> dry deposition velocities ( $\bar{v}_d$ ) from the observations, using:

$$\bar{v}_d = \frac{F_d}{[\text{Hg}^0]}$$

$\bar{F}_d$  is the measured litterfall or total foliar uptake flux and  $[\text{Hg}^0]$  is the annual mean atmospheric Hg<sup>0</sup> concentration. The atmospheric Hg<sup>0</sup> concentrations are taken directly from the measurement study, when reported. Otherwise, we searched for nearby atmospheric measurement sites for the relevant time period in the Atmospheric Mercury Network (AMNet),<sup>34</sup> Canadian Air and Precipitation Monitoring Network (CAPMoN),<sup>35</sup> European Monitoring and Evaluation Programme (EMEP),<sup>36</sup> and Global Mercury Observation System (GMOS).<sup>37</sup> Hg<sup>0</sup> observations are generally reported in units of ng m<sup>-3</sup> at standard temperature and pressure (STP, 273 K and 1 atm), whereas litterfall measurements would have units of µg per m<sup>2</sup> per year based on local conditions. Therefore, we apply a temperature and pressure correction using MERRA-2 meteorological data<sup>38</sup> to adjust annual mean measured Hg<sup>0</sup> concentrations from STP to local conditions. The applied correction yields 3 to 39% decreases in Hg<sup>0</sup> concentrations at local conditions compared to STP.

In total, we determined dry deposition velocities at 92 sites based on litterfall measurements, at 33 sites based on total foliar uptake, and at one site based on micrometeorological measurements.<sup>26</sup> The micrometeorological measurements were downloaded online<sup>39</sup> and analyzed based on annual mean values of dry deposition fluxes and concentrations. The locations of these studies are shown in Fig. 1.

Several issues must be considered when comparing modelled Hg<sup>0</sup> dry deposition velocities with the different measurement datasets (Table 1). Litterfall measurements do

- Litterfall
- Litterfall, throughfall, & wet dep
- ★ Flux tower (Obrist et al., 2021)

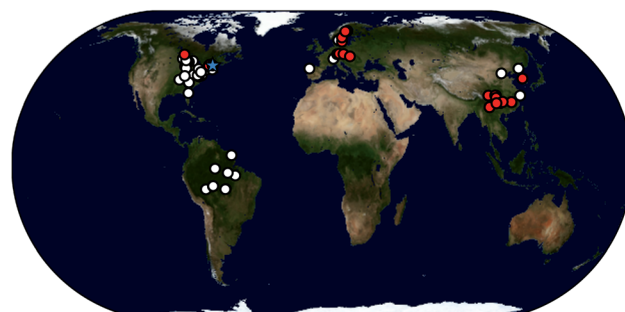


Fig. 1 Map showing locations of forest sites where Hg<sup>0</sup> vegetation uptake fluxes were measured in the compiled database.



not account for atmospheric  $\text{Hg}^0$  that is translocated from foliage into woody tissues, as well as additional uptake from lichens, mosses, and soils.<sup>6</sup> Therefore, we consider litterfall measurements to be a lower bound for total  $\text{Hg}^0$  dry deposition to a forest. Total foliar uptake measurements include an additional contribution from throughfall; however, throughfall fluxes include a fraction of previously dry deposited  $\text{Hg}^{2+}$  that is washed off the leaf surface, and thus may not be directly comparable with modelled  $\text{Hg}^0$  deposition. The contribution of  $\text{Hg}^{2+}$  dry deposition to throughfall likely varies spatially, with potentially higher contributions in areas close to anthropogenic  $\text{Hg}^{2+}$  emissions. One study in the Southeastern Tibetan Plateau region identified a 34–82% contribution from  $\text{Hg}^0$  to throughfall using isotopic evidence.<sup>25</sup> Micrometeorological measurements of net ecosystem  $\text{Hg}^0$  exchange may be the most accurate proxy of total  $\text{Hg}^0$  vegetation uptake.<sup>26</sup> Since net  $\text{Hg}^0$  exchange is measured, derived fluxes can include a negative contribution from soil  $\text{Hg}^0$  emissions; yet, Obrist *et al.*<sup>26</sup> did not find any periods of net  $\text{Hg}^0$  emissions from the forest floor during their study. Given the uncertainties of the comparison between modelled  $\text{Hg}^0$  dry deposition and Hg vegetation uptake measurements, we use other available measurements (*e.g.*, of atmospheric Hg concentrations) as an additional independent constraint on  $\text{Hg}^0$  dry deposition (Sections 3.2 and 3.3).

The exchange of Hg between the canopy and atmosphere is bi-directional;<sup>40</sup> all measurement methods studied here (litterfall, throughfall, and net ecosystem exchange) determine the net uptake flux rather than the gross uptake flux. The GEOS-Chem model does not explicitly include a parametrization for re-emission of  $\text{Hg}^0$  from foliar surfaces, so the modelled deposition fluxes should also be considered as net fluxes. GEOS-Chem calculates  $\text{Hg}^0$  emission fluxes from soil separately from the dry deposition scheme, using a parametrization depending on solar radiation and soil Hg concentration.<sup>16</sup>

## 2.2 GEOS-Chem description

We employ version 12.8.1 of the chemical transport model GEOS-Chem, whose Hg simulation is described by Horowitz *et al.*<sup>2</sup> We run the mercury simulation globally at  $2.0^\circ \times 2.5^\circ$  resolution and 47 vertical layers. The model's atmospheric transport is driven by MERRA-2 assimilated meteorological data.<sup>38</sup> The model calculates atmospheric mercury transport in three tracers: elemental mercury,  $\text{Hg}^0$ , divalent mercury,  $\text{Hg}^{2+}$ , and particulate-bound divalent mercury,  $\text{Hg}^{\text{P}}$ . Most of the simulations in this study use the GEOS-Chem v12.8.1 Hg chemical scheme, which considers bromine (Br) to be the primary  $\text{Hg}^0$  oxidant<sup>2</sup> and employs monthly mean Br oxidant concentrations from Schmidt *et al.*<sup>41</sup> Additional simulations (see Section 2.4 and Table 2) were conducted in version 12.8.1 of GEOS-Chem but with the new Hg chemical mechanism from Shah *et al.*<sup>3</sup> In the updated chemical mechanism, new reactions were added for the two-step oxidation of  $\text{Hg}^0$  to  $\text{Hg}^{2+}$  and the photolysis of gas phase  $\text{Hg}^+$  and  $\text{Hg}^{2+}$  compounds, based on new laboratory and computational data.<sup>42,43</sup> Whereas Br was the primary  $\text{Hg}^0$  oxidant in the prior chemical scheme,<sup>2</sup> Br and hydroxyl (OH) radicals play comparable roles in the net

oxidation of  $\text{Hg}^0$  in the new chemical scheme.<sup>3</sup> Shah *et al.*<sup>3</sup> also use updated Br oxidant fields that include the effect of sea-salt aerosol debromination and correct issues with heterogeneous recycling of Br radicals.<sup>44</sup> In both chemical mechanisms, aqueous reduction of  $\text{Hg}^{2+}$  to  $\text{Hg}^0$  is parametrized as a function of the  $\text{NO}_2$  photolysis rate and organic aerosol concentration, with a tuning parameter employed to optimize agreement with  $\text{Hg}^0$  observations.<sup>2</sup> Partitioning between gaseous and particulate  $\text{Hg}^{2+}$  is calculated according to Amos *et al.*<sup>45</sup> as a function of temperature and mass concentration of fine particulate matter (PM2.5). Wet deposition removes  $\text{Hg}^{2+}$  and  $\text{Hg}^{\text{P}}$  from the atmosphere according to gas<sup>45</sup> and particulate<sup>46</sup> parametrizations.

The  $\text{Hg}^0$  dry deposition scheme in GEOS-Chem uses a resistance-based approach,<sup>19,20</sup> similar to many other chemical transport models.<sup>15,18</sup> Dry deposition is parametrized assuming three types of resistances in series: aerodynamic, boundary, and surface resistance. Aerodynamic and boundary resistances depend on grid scale meteorological variables (*e.g.*, temperature and windspeed), whereas surface resistance depends on the land use category, surface parameters (*e.g.*, leaf area index, LAI), chemical compound-specific parameters, and meteorology. The surface resistance is determined by calculating the effect of parallel resistances of vegetation stomata, cuticles, lower canopy surfaces, and the ground surface (including soil and leaf litter). To incorporate compound-specific effects, the Henry's law constant ( $H^*$ ) and biological reactivity ( $f_0$ ) of a compound are used as scaling factors in the resistance calculations (see Section S1† for full set of equations included in the dry deposition model). Compounds that are more soluble (higher  $H^*$ ) and/or more biologically reactive (higher  $f_0$ ) have faster dry deposition velocities,<sup>20</sup> since dissolution and reaction are two parallel pathways for deposition to surfaces (Section S1†). A grid cell in GEOS-Chem can contain multiple land use categories; the dry deposition velocity is computed separately for each land use category within a grid cell and then averaged with area-weighting to produce the overall dry deposition velocity in a grid cell.

The implementation of dry deposition in GEOS-Chem uses 11 land use categories, with the categories relevant to this paper being deciduous forests, coniferous forests, and tropical rainforests.<sup>47</sup> Since information about grid surface parameters in GEOS-Chem (*e.g.*, LAI) is grouped into 73 land use categories according to Gibbs,<sup>48</sup> for the dry deposition scheme each of the 73 land categories is assigned to one of the 11 dry deposition categories. We use a reprocessed version of the Moderate Resolution Imaging Spectroradiometer (MODIS) LAI product<sup>49</sup> in the dry deposition scheme. For  $\text{Hg}^0$  in GEOS-Chem,  $H^*$  is set to  $0.11 \text{ M atm}^{-1}$  (ref. 50) and  $f_0$  was originally set to  $10^{-5}$  to match the observations over North America available at the time.<sup>51</sup> Over the ocean,  $\text{Hg}^0$  dry deposition is calculated as part of the air-sea gas exchange model<sup>52</sup> instead of through the resistance-based scheme. Gaseous  $\text{Hg}^{2+}$  is biologically unreactive ( $f_0 = 0$ ) but highly soluble ( $H^* = 10^{14} \text{ M atm}^{-1}$ ) and the dry deposition of particulate Hg is calculated according to aerosol deposition scheme.<sup>53,54</sup>



Table 2 Description of GEOS-Chem Hg simulations

| Simulation name | Description  | $Hg^0$ biological reactivity ( $f_0$ )                        | Reduction coefficient <sup>a</sup> ( $\alpha$ ) |
|-----------------|--|---|---|
| BASE            | Reference GEOS-Chem version 12.8.1   | $10^{-5}$   | 0.16  |
| OBRIST          | Matching flux tower measurements at Harvard Forest <sup>26</sup>                                       | $3 \times 10^{-5}$  | 0.16  |
| OBRIST_R        | Matching Obrist <i>et al.</i> <sup>26</sup> measurements; increased $Hg^{2+}$ reduction                | $3 \times 10^{-5}$  | 0.33  |
| AMAZON_L        | Lower bound for Amazon: matching Hg litterfall flux from sites in Fostier <i>et al.</i> <sup>31</sup>  | $9 \times 10^{-5}$ (Amazon)<br>$3 \times 10^{-5}$ (elsewhere) | 0.33  |
| AMAZON_U        | Upper bound for Amazon: matching total foliar uptake of Hg from Fostier <i>et al.</i> <sup>31,90</sup> | 0.2 (Amazon)<br>$3 \times 10^{-5}$ (elsewhere)                | 0.33  |
| NEWCHEM         | Reference GEOS-Chem simulation based on new Hg chemical scheme from Shah <i>et al.</i> <sup>3</sup>    | $10^{-5}$   | 0.004 <sup>b</sup>                              |
| NEWCHEM_D       | Increasing dry deposition to parameters from AMAZON_U; new chemistry <sup>3</sup>                      | 0.2 (Amazon)<br>$3 \times 10^{-5}$ (elsewhere)                | 0.010 <sup>b</sup>                              |

<sup>a</sup> In GEOS-Chem, the photoreduction rate of aqueous-phase  $Hg^{2+}$ -organic complexes is parametrized as  $\alpha j_{NO_2} [OA] [Hg^{2+}(aq)]$ , where  $\alpha$  is a tuned coefficient,  $j_{NO_2}$  is the local photolysis rate of  $NO_2$ , and  $[OA]$  is the mass concentration of organic aerosol at STP. <sup>b</sup> In the new chemical scheme, photoreduction of aqueous  $Hg^{2+}$ -organic complexes is parametrized differently, as  $\alpha j_{NO_2} [Hg^{2+}P(\text{org})]$ , where  $[Hg^{2+}P(\text{org})]$  is the concentration of particulate  $Hg^{2+}$ -organic complexes. Thus, the  $\alpha$  coefficients cannot be directly compared with earlier GEOS-Chem versions.

Gridded emissions from anthropogenic sources are based on the 2015 inventory<sup>55,56</sup> prepared for the 2018 Global Mercury Assessment.<sup>1</sup> All other emissions follow Horowitz *et al.*<sup>2</sup> Monthly mean surface ocean Hg concentrations are taken from Horowitz *et al.*,<sup>2</sup> based on two-way coupling of GEOS-Chem with the MITgcm 3-D mercury ocean model.<sup>57</sup> To account for prompt recycling of  $Hg^{2+}$ , 20% of  $Hg^{2+}$  wet and dry deposition to terrestrial surfaces are re-emitted to the atmosphere as  $Hg^0$  directly after depositing.<sup>51</sup>

### 2.3 Offline dry deposition model

We ported the GEOS-Chem dry deposition code to Python so that it could be run with meteorological inputs in offline calculations (<https://doi.org/10.5281/zenodo.6498126>). This offline model enables quicker simulations of dry deposition velocities than running the full online chemistry-transport model. The inputs to the model are hourly MERRA2 meteorological data for 2015 (including temperature, wind speed, cloud fraction, radiation fluxes), land surface information for the 73 land categories,<sup>48</sup> and weekly-averaged satellite-derived LAI maps for 2015.<sup>49</sup> The output of the offline model is hourly dry deposition velocity maps for 2015. With an hourly time resolution for meteorological inputs, the offline model shows small enough errors for the current study application compared to online GEOS-Chem velocities (mean grid cell error  $\sim 0.1\%$ ) (ESI,<sup>†</sup> Section S2).

In this study, we run offline simulations with the biological reactivity ( $f_0$ ) of  $Hg^0$  varying from  $10^{-5}$  to 1 and compare the resultant deposition velocity maps with the observational database. We focus on uncertainties in  $f_0$  since this parameter covers multiple potential biological reaction processes in vegetation uptake and therefore would be difficult to determine experimentally. In GEOS-Chem,  $f_0$  of  $Hg^0$  has been set to  $10^{-5}$  based on Selin *et al.*,<sup>51</sup> yet other modelling exercises use a higher  $Hg^0$  biological reactivity of 0.1 and 0.2.<sup>58,59</sup> We chose to vary the chemical compound-specific parameter  $f_0$  instead of general resistance parameters within the dry deposition scheme, since

the resistance parameters have been validated in model comparisons with other chemical compounds<sup>60</sup> and would require a wider scope of chemical compounds measurements to evaluate (see Section S5<sup>†</sup> for further discussion).

The compiled observations are made at forest sites, whereas the corresponding model grid cells ( $2.0^\circ \times 2.5^\circ$ ) can cover multiple land types. We account for the specific land use category of the observation site in the offline model calculations following an approach by Silva and Heald.<sup>60</sup> To do so, we categorize each observation site within the 11 land type categories used in the dry deposition scheme (e.g., broadleaf, coniferous, and tropical rain forest). We alter the offline model's inputs so that the land type at the observation site accounts for 100% of the model grid cell. The LAI of the grid cell is set to the average LAI of the observed forest category within the grid cell. The surface roughness of the grid cell is adjusted to 1 m when it drops below that threshold, since 1 m is representative of forested areas.<sup>61</sup> We present the effects of the land-surface adjustment in the ESI (Section S3<sup>†</sup>). In the case of  $Hg^0$ , this adjustment is especially important for coastal grid cells, where the low deposition velocity over the water-covered sub-grid cell reduces the overall grid cell deposition velocity.

### 2.4 GEOS-Chem simulations

We conducted a four-year spinup of the GEOS-Chem Hg model (2010–2013) to create initial conditions for the subsequent simulations. Based on the comparison between the offline dry deposition model and observations (presented in Section 3.1), we ran two-year online simulations (2014–2015) for the different dry deposition settings (Table 2). Allowing for a one-year equilibration in the troposphere, we analyze year 2015 in the simulations. A reference BASE simulation ( $f_0 = 10^{-5}$ ) is conducted with GEOS-Chem version 12.8.1. Three more simulations with different  $f_0$  parameter values were run: an OBRIST simulation with  $f_0$  set to  $3 \times 10^{-5}$  globally, as well as simulations where  $f_0$  is increased regionally in the Amazon rainforest



to  $9 \times 10^{-5}$  (AMAZON\_L simulation) and 0.2 (AMAZON\_U simulation) and set to  $3 \times 10^{-5}$  elsewhere.

In order to balance the enhanced removal of  $\text{Hg}^0$  due to dry deposition in the OBRIST simulation, we adjust the reduction rate of  $\text{Hg}^{2+}$  to match annual mean observations of atmospheric  $\text{Hg}^0$  concentrations in the Northern Hemisphere in the OBRIST\_R simulation. The larger reduction rate coefficient is also used in the AMAZON\_L and AMAZON\_U simulations. The  $\text{Hg}^{2+}$  reduction rate coefficient has been used as a tuning parameter in past developments of the GEOS-Chem model.<sup>2,3</sup> Furthermore, here we have applied an offline three-box atmospheric model to reduce the computational expense of tuning the reduction rate (Section S4†).

To compare the effects of increased  $\text{Hg}^0$  dry deposition in the updated Hg chemistry mechanism,<sup>3</sup> we run a reference simulation for the updated chemistry (NEWCHEM), as well as a simulation accounting for higher  $\text{Hg}^0$  dry deposition globally ( $f_0 = 3 \times 10^{-5}$ ) and in the Amazon ( $f_0 = 0.2$ ) and faster aqueous  $\text{Hg}^{2+}$  reduction (NEWCHEM\_D) (Table 2). All emission settings remain unchanged from earlier simulations (Section 2.2).

As an illustrative scenario, we investigate the impact of the Amazon transitioning from rainforest to savannah (*savannization*) on the global vegetation uptake of Hg and the atmospheric Hg budget in GEOS-Chem. We follow the approach used by Alves de Oliveira *et al.*<sup>62</sup> as a worst-case scenario for Amazon savannization due to deforestation and climate change. To set up the simulation, we replace all tropical rain forest land cover in South America with savanna land cover. We substitute Amazon LAI with mean time-varying LAI from current savanna areas in South America. Since the Hg budget of the savannization simulation is compared to AMAZON\_U,  $f_0$  is set to  $3 \times 10^{-5}$  (no rainforest is present in Amazon, so the regional  $f_0$  setting is not applied).

### 3. Results and discussion

#### 3.1 Comparison of offline model with vegetation uptake measurements

We compare the dry deposition velocities predicted by the offline model simulations to observations of litterfall (separating outside and inside the Amazon), total foliar uptake, and flux tower measurements (Fig. 2). The interquartile range of  $\text{Hg}^0$  dry deposition velocities predicted by the BASE version of GEOS-Chem ( $f_0 = 10^{-5}$ ),  $0.035\text{--}0.039 \text{ cm s}^{-1}$ , matches well with litterfall measurements outside the Amazon,  $0.020\text{--}0.041 \text{ cm s}^{-1}$  (Fig. 2). These measurements are located in mainly temperate and boreal forests in North America, Europe, and East Asia. Previous studies have also found good agreement between GEOS-Chem  $\text{Hg}^0$  dry deposition and a USA subset of litterfall measurements.<sup>9,16</sup> When the throughfall dry deposition component is added to litterfall, the median dry deposition velocity of observations increases by  $\sim 36\%$ , from  $0.028 \text{ cm s}^{-1}$  to  $0.038 \text{ cm s}^{-1}$ . The interquartile ranges of BASE ( $0.034\text{--}0.041 \text{ cm s}^{-1}$ ) also overlap with total foliar uptake observations ( $0.030\text{--}0.055 \text{ cm s}^{-1}$ ). The modelled dry deposition velocity at Harvard Forest ( $0.038 \text{ cm s}^{-1}$ ) underpredicts the flux tower measured value<sup>26</sup> ( $0.072 \text{ cm s}^{-1}$ ) by a factor of 1.9. Even larger

underestimates are seen when comparing the BASE model to deposition velocities derived from Amazon litterfall ( $-72\%$  from observation median) and Amazon total foliar uptake ( $-87\%$  from observation median).<sup>31</sup>

When the value of  $f_0$  is adjusted to  $3 \times 10^{-5}$  (OBRIST simulation), the model matches the  $\text{Hg}^0$  deposition velocity derived from the flux tower measurements. In this case, the model overestimates median total foliar uptake deposition velocities by 78%. This model-based estimate is only based on one flux tower measurement site, and more flux tower measurements of  $\text{Hg}^0$  exchange over forests would be necessary to confirm the stronger sink measured by Obrist *et al.*<sup>26</sup> Nevertheless, the larger dry deposition velocities measured by flux tower measurements compared to litterfall could be explained by litterfall measurements not accounting for uptake from woody tissues, lichens and mosses.<sup>6</sup>

The model continues to underestimate Amazon litterfall measurements when  $f_0$  of  $\text{Hg}^0$  is set globally to  $3 \times 10^{-5}$  (OBRIST) (Fig. 2). A previous study with a different atmospheric Hg model that uses a resistance-based approach to dry deposition (GEM-MACH-Hg) also underestimated deposition fluxes inferred from tropical rainforest litterfall measurements.<sup>5</sup> We therefore applied a new regional  $f_0$  parameter for the rainforest land type in South America. Setting  $f_0$  to  $9 \times 10^{-5}$  within only the Amazon rainforest and retaining  $f_0 = 3 \times 10^{-5}$  elsewhere (AMAZON\_L simulation), leads to a match for the Amazon litterfall deposition velocity ( $0.17 \text{ cm s}^{-1}$ ). We take this value as a lower bound estimate for  $\text{Hg}^0$  dry deposition in the Amazon, since litterfall does not account for all vegetation uptake (Table 1). As an upper bound estimate for the Amazon dry deposition velocity, we use the total foliar uptake estimate, litterfall + throughfall – open field wet deposition ( $49 + 72 - 18 = 103 \mu\text{g per m}^2 \text{ per year}$ ), reported by Fostier *et al.*<sup>31</sup> Dividing this by the atmospheric  $\text{Hg}^0$  concentration measured in the GMOS station at Manaus, we calculate a deposition velocity of  $0.35 \text{ cm s}^{-1}$ . This estimate is considered an upper bound for Amazon  $\text{Hg}^0$  uptake since lower throughfall fluxes ( $13.7\text{--}23.6 \mu\text{g per m}^2 \text{ per year}$ ) have been reported for other regions of the Brazilian Amazon.<sup>63</sup> A recent study from the Peruvian Amazon measured a slightly higher total foliar uptake flux ( $128 \mu\text{g per m}^2 \text{ per year}$ ); however, the study area is impacted by regional artisanal and small-scale gold mining (ASGM) emissions.<sup>64</sup> The upper observed bound of Amazon dry deposition velocity from Fostier *et al.*<sup>31</sup> would correspond to a  $f_0$  value of 0.2 (AMAZON\_U simulation).

Instead of altering  $f_0$ , another approach to adjusting the  $\text{Hg}^0$  dry deposition velocity for the Amazon rainforest would have been to alter the dry deposition canopy resistances for the rainforest land category. We show that an equivalent solution for  $\text{Hg}^0$  deposition in the Amazon can be found by adjusting resistances (Section S5†). However, since adjusting resistances would affect all dry depositing compounds in GEOS-Chem and perturb their atmospheric budgets, for this study we proceeded with adjustments to the  $\text{Hg}^0$ -specific parameter,  $f_0$ . Given that both approaches would yield the same  $\text{Hg}^0$  dry deposition velocities, the choice of approach should not affect the subsequent GEOS-Chem analyses in this study. Nevertheless, this



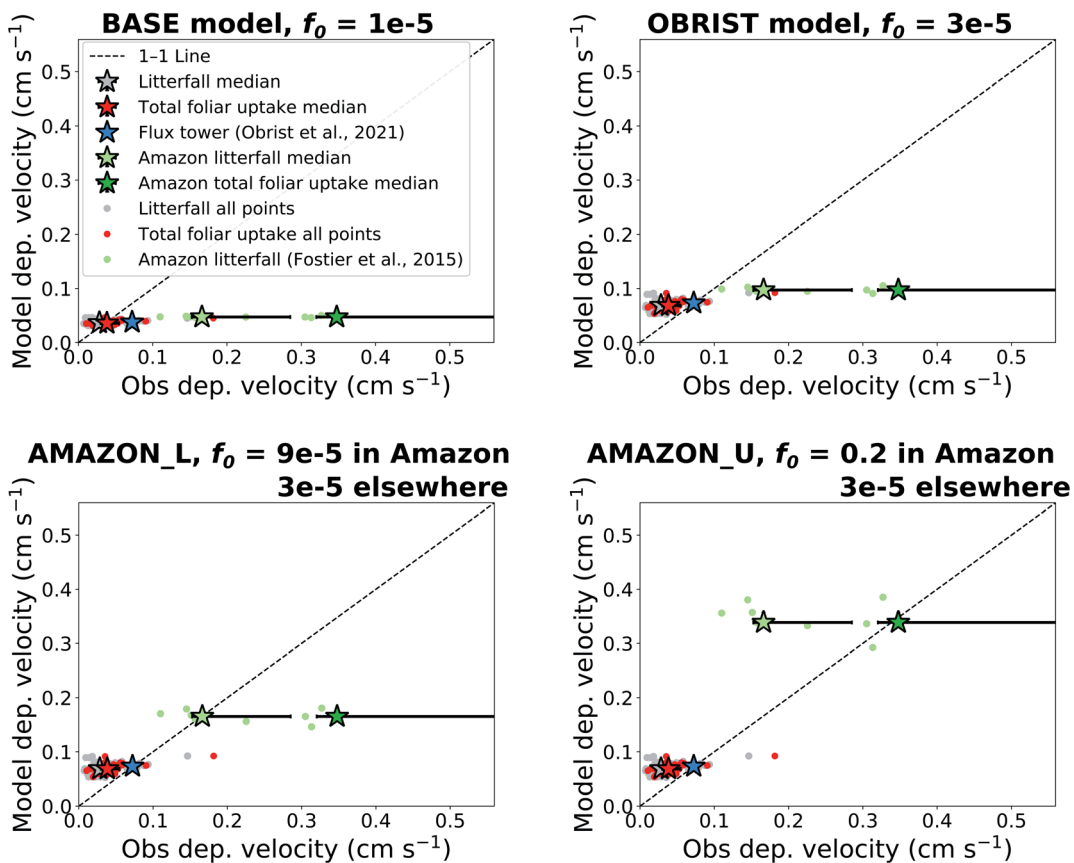


**Fig. 2** Comparing observed dry deposition velocities with modelled values extracted from the location coordinates. Four offline model settings are presented, with varying assumptions for the biological reactivity ( $f_0$ ) of  $\text{Hg}^0$  in the dry deposition scheme. Individual site measurements are indicated with filled circles and overall medians of measurement types are indicated with filled stars. Error bars show the interquartile range of measurements over different measurement locations. Model interquartile ranges are generally smaller than the size of the markers.

issue should be revisited with a more extensive comparison of multiple chemical compounds, as GEOS-Chem (Section S5†) and another model with a resistance-based approach<sup>65</sup> have also been found to underestimate the ozone dry deposition velocity in the Amazon.

### 3.2 Seasonality of atmospheric $\text{Hg}^0$

We compare the atmospheric  $\text{Hg}^0$  seasonal cycle from online GEOS-Chem simulations (Table 2) with observations in Fig. 3. Under the BASE simulation, GEOS-Chem is within the  $1\sigma$  spatial variability of Northern Hemisphere (NH) midlatitude observations in all months except April (Fig. 3a). However, the seasonal amplitude of the BASE model ( $0.17 \text{ ng m}^{-3}$ ) is only half the observed seasonal amplitude ( $0.34 \text{ ng m}^{-3}$ ), showing a weaker summertime minimum in total gaseous mercury (TGM). In the BASE version of GEOS-Chem, seasonality in Hg oxidation drives the summertime minimum in the NH.<sup>2,66</sup> In the OBRIST simulation, with increased  $\text{Hg}^0$  dry deposition, the model's seasonal amplitude ( $0.28 \text{ ng m}^{-3}$ ) is closer to observations ( $0.34 \text{ ng m}^{-3}$ ) although the mean concentrations are biased low compared to observations. This bias can be offset by adjusting the reduction of  $\text{Hg}^{2+}$  to  $\text{Hg}^0$  in organic aerosol, which has been done to tune previous GEOS-Chem Hg model versions.<sup>2,3</sup> The OBRIST\_R

simulation illustrates that when the  $\text{Hg}^{2+}$  reduction rate coefficient is increased by a factor of 2.1, the model based on flux tower measurements can match both the mean (within  $1\sigma$ ) and the seasonal amplitude of observed  $\text{Hg}^0$  in the NH midlatitudes (Fig. 3a). More information about the tuning procedure for Hg reduction, as well as comparisons with observed  $\text{Hg}^0$  concentrations globally, can be found in the ESI† (Section S4 and Fig. S9†).

The improved agreement of the modelled seasonal cycle upon increasing the strength of  $\text{Hg}^0$  dry deposition supports previous work suggesting that the  $\text{Hg}^0$  seasonal cycle in the NH is driven mainly by the vegetation sink, not oxidation chemistry.<sup>4,5</sup> The simulations that further increase Amazon uptake of  $\text{Hg}^0$  (AMAZON\_L and AMAZON\_U) are similar in seasonality to the OBRIST\_R simulation in the NH midlatitudes. Thus, the three simulations OBRIST\_R, AMAZON\_L, and AMAZON\_U can all be compatible with NH midlatitude  $\text{Hg}^0$  observations and suggest that the vegetation uptake in the BASE model is too small.

Shah *et al.*<sup>3</sup> updated the Hg chemical scheme in GEOS-Chem (NEWCHEM), leading to substantial differences in the seasonal cycle of TGM in the NH midlatitudes (Fig. 3a). In the NEWCHEM simulation, the minimum  $\text{Hg}^0$  concentrations occur in



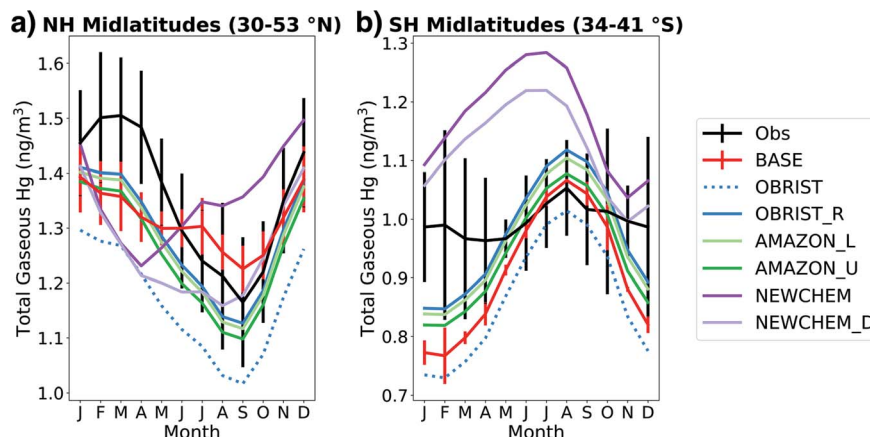


Fig. 3 Seasonal cycle of surface total gaseous mercury (TGM) concentrations in the (a) Northern Hemisphere (NH) midlatitudes (16 observation stations) and (b) Southern Hemisphere (SH) midlatitudes (3 observation stations). Lines indicate monthly means of simulated or observed  $\text{Hg}^0$  at station locations and error bars indicate standard deviations between measurement sites. To improve plot clarity, model error bars are only shown for the BASE simulation. Measured atmospheric Hg concentrations are sourced from compilations<sup>18,91</sup> and are courtesy of Hélène Angot.

April, whereas BASE chemistry leads to a minimum in September. This difference is caused by the seasonality of Br oxidant concentrations; NEWCHEM uses updated Br fields<sup>44</sup> that show maximum concentrations in the NH in late winter–spring, whereas the Br fields used by BASE<sup>41</sup> are maximum in summer. When dry deposition is enhanced in the new chemistry version (NEWCHEM\_D), the minimum TGM concentration is shifted to August, closer to observations. The seasonal amplitude of NEWCHEM\_D ( $0.25 \text{ ng m}^{-3}$ ) is similar to the updated simulations using the previous chemical mechanism (OBRIST\_R, AMAZON\_L, and AMAZON\_U), illustrating that NH midlatitude TGM seasonality can be a useful constraint for  $\text{Hg}^0$  dry deposition.<sup>4</sup> However, NEWCHEM\_D still shows too low TGM concentrations throughout the boreal spring (March–May), suggesting that further investigation into the uncertainties of atmospheric Hg chemistry is required.

In the Southern Hemisphere (SH) midlatitudes, the observations show a relatively flat seasonal cycle in  $\text{Hg}^0$  (amplitude of  $0.09 \text{ ng m}^{-3}$ ) (Fig. 3b). Jiskra *et al.*<sup>4</sup> have attributed this lack of seasonality to less land area in the SH, and thus a more minor vegetation sink. In contrast, the BASE version of GEOS-Chem shows a strong seasonal cycle (amplitude of  $0.30 \text{ ng m}^{-3}$ ), with a wintertime maximum and summertime minimum likely driven by oxidation chemistry.<sup>2,3</sup> The seasonal amplitude is largely unchanged ( $0.29 \text{ ng m}^{-3}$ ) when dry deposition is increased in the OBRIST simulation, because of the limited influence of land in the SH. When the reduction of  $\text{Hg}^{2+}$  is increased in OBRIST\_R, the seasonality is slightly flattened, with an amplitude of  $0.27 \text{ ng m}^{-3}$ . Further adjustments to the Amazon dry deposition flux (AMAZON\_L and AMAZON\_U) lead to reductions in mean SH midlatitude TGM, but limited changes in seasonal amplitude. Simulations with the new chemical mechanism (NEWCHEM and NEWCHEM\_D) also show too strong TGM seasonality in the SH (amplitudes of  $0.22$  and  $0.25 \text{ ng m}^{-3}$ ) and generally overestimate SH midlatitude concentrations (annual mean bias of  $+0.18$  and  $+0.13 \text{ ng m}^{-3}$ ).

Uncertainties with the GEOS-Chem Hg chemical scheme as well as seasonality of Br oxidant concentrations could be responsible for the bias in TGM seasonality in the SH.<sup>3</sup> A further uncertainty is the seasonality of  $\text{Hg}^0$  emissions from the ocean, which would likely be a dominating source in the SH.<sup>2</sup>

### 3.3 Atmospheric $\text{Hg}^0$ in South America

Previous validations of GEOS-Chem<sup>2,3,66</sup> have paid limited attention to South America, where until now very few measurements were available. Given the importance of the Amazon region as an area of dry deposition (accounting for 29% of the global  $\text{Hg}^0$  dry deposition to land in AMAZON\_U), we evaluate GEOS-Chem results against recent atmospheric Hg measurements from South America<sup>37,67,68</sup> (Fig. 4). Atmospheric  $\text{Hg}^0$  observations from Chacaltaya, a mountain-top observatory in the Bolivian Andes, showed an increasing trend between normal (July 2014–May 2015) and El-Niño Southern Oscillation (ENSO) conditions (June 2015–February 2016).<sup>67</sup> We focus our comparison on normal conditions at Chacaltaya, since the  $\text{Hg}^0$  ocean emissions in GEOS-Chem would not be representative of ENSO conditions.<sup>2</sup> In general, Hg concentrations measured in stations surrounded by tropical rainforest (Manaus, Suriname, and Chacaltaya) are all overestimated by the BASE version of GEOS-Chem (BASE mean over stations:  $1.27 \text{ ng m}^{-3}$  vs. observed mean:  $1.03 \text{ ng m}^{-3}$ ). Only at the midlatitude site Bariloche, which would be less affected by the Amazon vegetation uptake sink, is the BASE model within the measurement  $1\sigma$  variability. Passive Hg samplers, as part of the Latin American Passive Air sampling Network (LAPAN) network, are a new source of information for Hg cycling in South America.<sup>68</sup> We compare the mean of passive-sampler measured annual Hg concentrations from 22 background locations in South America with model simulations (Fig. 4). The BASE simulation also overestimates the mean Hg concentration from the passive sampler network ( $1.14 \text{ ng m}^{-3}$  vs.  $0.87 \text{ ng m}^{-3}$ ), supporting the comparison with other measurement stations.



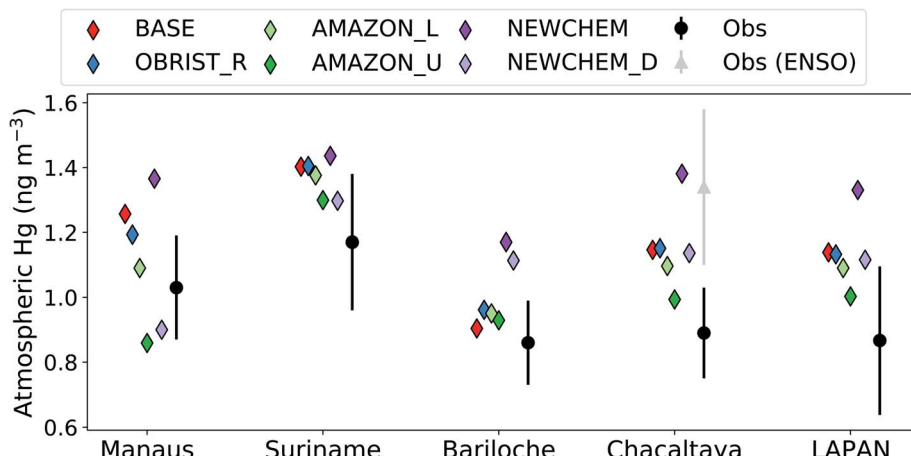


Fig. 4 Comparing GEOS-Chem simulations to available South American observations of atmospheric Hg (LAPAN stands for Latin American Passive Sampling Network). Total gaseous mercury (TGM) concentrations for simulations and observations are compared at each site, except for Suriname for which gaseous  $\text{Hg}^0$  (GEM) concentrations are compared. Error bars for observations indicate the  $1\sigma$  temporal variability, except for LAPAN which shows the  $1\sigma$  spatial variability between 22 sites.

The OBRIST\_R simulation with increased  $\text{Hg}^0$  biological reactivity globally remains outside the measurement  $1\sigma$  variability at South American sites, except for the midlatitude site Bariloche. With the adjustment to Amazon  $\text{Hg}^0$  biological reactivity in AMAZON\_L and AMAZON\_U, the bias in GEOS-Chem predictions are generally reduced at the South American sites (Fig. 4). Overall, the AMAZON\_U simulation seems to agree best with  $\text{Hg}^0$  measurements, lying within the  $1\sigma$  variability at all measurement sites except for Manaus, where the AMAZON\_L simulation is closest. Our comparison with observations of atmospheric  $\text{Hg}^0$  concentrations in South America supports the conclusion that the vegetation uptake of Hg in the Amazon is currently underestimated in GEOS-Chem. In addition to dry deposition uncertainties, atmospheric Hg concentrations over South America may also be affected by uncertainties in soil re-emissions, artisanal and small-scale gold mining emissions, air-sea exchange, and volcanic emissions.<sup>1,15,67</sup> Nevertheless, correcting GEOS-Chem to be in line with Amazon litterfall and throughfall data, helps reduce the South American  $\text{Hg}^0$  bias in GEOS-Chem from  $+0.21 \text{ ng m}^{-3}$  (BASE) to  $+0.05 \text{ ng m}^{-3}$  (AMAZON\_U), averaged over the observations in Fig. 4. The new Hg chemical scheme,<sup>3</sup> generally leads to higher Hg concentrations in the SH (Fig. 3b and 4). However, as with the old chemical scheme,<sup>2</sup> we find that the enhancement of dry deposition globally and over the Amazon improves the overall South American  $\text{Hg}^0$  bias from  $+0.37 \text{ ng m}^{-3}$  (NEWCHEM) to  $+0.15 \text{ ng m}^{-3}$  (NEWCHEM\_D).

#### 3.4 Wet deposition fluxes of Hg

An additional observational constraint on atmospheric Hg cycling is measured wet deposition fluxes. Due to the relative insolubility of  $\text{Hg}^0$ , wet deposition fluxes depend on the atmospheric concentrations of  $\text{Hg}^{2+}$ . Our adjustments to increase the  $\text{Hg}^0$  dry deposition to land consequently result in less available

$\text{Hg}^0$  for oxidation and thus decrease the wet removal sink of  $\text{Hg}^{2+}$ . The BASE version of GEOS-Chem underestimates observed annual mean wet deposition globally ( $7.5 \mu\text{g m}^{-2}$  vs.  $8.3 \mu\text{g m}^{-2}$ , Fig. S10†). The mean simulated wet deposition decreases in AMAZON\_U ( $4.5 \mu\text{g m}^{-2}$ ), increasing the model bias. However, other processes may explain the deviation between GEOS-Chem and wet deposition measurements. For example, GEOS-Chem underestimates  $\text{Hg}^{2+}$  in the free troposphere, likely due to uncertainties in atmospheric Hg oxidation, leading to less Hg removal by convective storms.<sup>3,69</sup> Indeed, when the new chemistry scheme is applied from Shah *et al.*<sup>3</sup> (NEWCHEM\_D), Hg wet deposition increases over Europe compared to AMAZON\_U ( $4.8 \mu\text{g m}^{-2}$  vs.  $3.4 \mu\text{g m}^{-2}$ , Fig. S12†), but remains too low globally ( $4.9 \mu\text{g m}^{-2}$ , Fig. S10†). Other studies have cited the difficulty of resolving  $\text{Hg}^{2+}$  hotspots and transport in global models,<sup>70,71</sup> the speciation of anthropogenic Hg emissions,<sup>33,72</sup> and the lack of Hg in coarse particles in GEOS-Chem<sup>73</sup> as possible reasons for the wet deposition underestimation. Further analysis and observational constraints are required to investigate the influence of these uncertainties on Hg wet deposition.

#### 3.5 Importance of Amazon rainforest as a $\text{Hg}^0$ sink

Both litterfall flux and atmospheric  $\text{Hg}^0$  concentration measurements suggest that the Amazon rainforest is currently an important net  $\text{Hg}^0$  sink, yet this sink is at risk due to continued deforestation and climate change.<sup>14,74</sup> Two tipping points have been suggested that could cause the rainforest to transition into a savannah biome: a temperature increase of  $4^\circ\text{C}$  above preindustrial or 20–40% deforestation in the region.<sup>75</sup> Once these thresholds are crossed, regional moisture recycling weakens to the extent that there is not enough available water to support tropical rainforest biomes.

To investigate the effect of Amazon savannization on regional and global Hg cycling, we simulated an extreme



scenario where the entire Amazon rainforest is converted to savannah land cover, following the approach of Alves de Oliveira *et al.*<sup>62</sup> In the AMAZON\_U simulation, median modelled Hg<sup>0</sup> dry deposition velocities in the Amazon rainforest are 0.3 cm s<sup>-1</sup>, while in the savannah scenario this decreases to 0.07 cm s<sup>-1</sup> (Fig. 5a). Correspondingly, the Hg<sup>0</sup> dry deposition over the Amazon region decreases by 63% in the savannah scenario (Fig. 5b), from 653 Mg per year to 246 Mg per year. Total Hg deposition to the ocean increases by 283 Mg per year, mostly spread evenly across the SH but with an intensified band in the eastern equatorial Pacific. In the absence of the Amazon rainforest uptake sink, the total Hg burden in the atmosphere increases by 194 Mg (+5%) compared to current conditions.

In South America, the major direct anthropogenic source of Hg is from ASGM, emitting 340 Mg per year to the atmosphere.<sup>1</sup> Much of the ASGM activities occur within the Amazon region.<sup>76,77</sup> Due to uptake of Hg by vegetation, terrestrial ecosystems close to ASGM sources are threatened by high Hg exposures.<sup>64</sup> The ASGM Hg<sup>0</sup> emissions may change in the future as parties to the Minamata Convention on Mercury are obligated to take steps to reduce Hg use in ASGM.<sup>78</sup> To check how much of the rainforest Hg<sup>0</sup> sink is caused by regional emissions, we ran two scenarios with no South American anthropogenic Hg emissions and either existing rainforest conditions or full savannah conversion. Even when regional emissions are removed, savannization results in an additional 238 Mg per year Hg transferred to the ocean (83% of the effect calculated with current South American emissions). The Amazon rainforest is thus not only a sink of regional Hg but also global background Hg, due to the long atmospheric lifetime of Hg<sup>0</sup>.

Previous work has identified several processes that mobilize Hg during Amazon deforestation.<sup>31</sup> Soil erosion and mobilization increases in deforested areas, with annual Hg mobilization expected to increase by 20–25% between 2014 and 2030 in a Peruvian watershed affected by deforestation.<sup>79</sup> Fires used to clear forested areas for agriculture have been estimated to emit 6.7 Mg Hg per year between 2000 and 2008 in the Brazilian Amazon.<sup>80</sup> Deforested areas also show higher soil Hg emissions than forested areas, with soils releasing an estimated 2.3 g per Hg per ha in the first year after the fire.<sup>7</sup> When scaled by the

estimated deforestation rate from the Brazilian Amazon in 2021 ( $1.3 \times 10^6$  ha per year),<sup>81</sup> the additional soil source after deforestation would correspond to 3.0 Mg Hg per year. With our current study, we quantified another process leading to increased mobilization of Hg to marine ecosystems: a decreased land sink that leads to additional Hg deposition to the ocean. The estimated increased Hg deposition flux to the ocean (283 Mg per year) represents two-thirds of the total anthropogenic South American emissions (340 Mg per year), emphasizing the importance of Amazon rainforest trends for future Hg contamination. This shift in Hg deposition from land to the ocean increases the overall mobility of Hg in the surface environment since Hg in soil reservoirs has a longer mean residence time than in the surface ocean.<sup>82</sup> Increased exposure to Hg health risks may not be limited to marine ecosystems, since deforestation can increase Hg methylation rates in freshwater aquatic ecosystems.<sup>83</sup> Efforts to mitigate climate change and avoid deforestation will be crucial to avoid additional mobilization of Hg in the environment, meaning that the goals of the Minamata Convention intersect with other international treaties such as the Paris Climate Accords.<sup>78</sup>

#### 4. Environmental and modelling implications

Fig. 6 illustrates the global atmospheric Hg budget under the original GEOS-Chem simulation BASE and the updated simulation AMAZON\_U (other simulation budgets are shown in Table S2†). The atmospheric Hg<sup>0</sup> burden (~3600 Mg) remains similar in both simulations, given that Hg<sup>2+</sup> reduction was increased to compensate for increased Hg<sup>0</sup> deposition in AMAZON\_U. Overall, dry deposition of Hg<sup>0</sup> to land approximately doubles from 1200 Mg per year in BASE to 2276 Mg per year in AMAZON\_U. The new global dry deposition flux to land (2276 Mg per year) lies in between the estimate from a previous global litterfall assessment (1180 Mg per year)<sup>27</sup> and the estimate extrapolated globally from one flux tower measurement site over a midlatitude forest (3490 Mg per year).<sup>26</sup> The new estimate from GEOS-Chem is within the lower end of the range ( $2705 \pm 504$  Mg per year) derived by a new assessment that

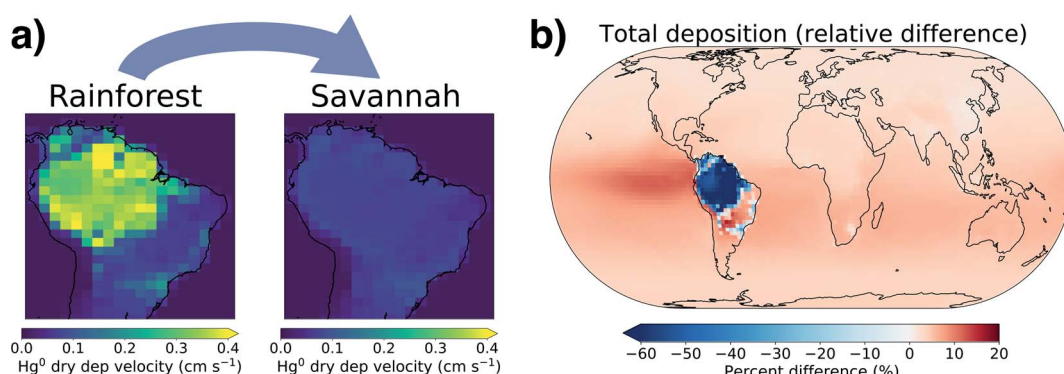


Fig. 5 (a) GEOS-Chem modeled Hg<sup>0</sup> dry deposition velocities shown for the Amazon under current land cover (left) and total conversion to savannah (right). (b) Map of the simulated change in total Hg deposition flux due to savannization.



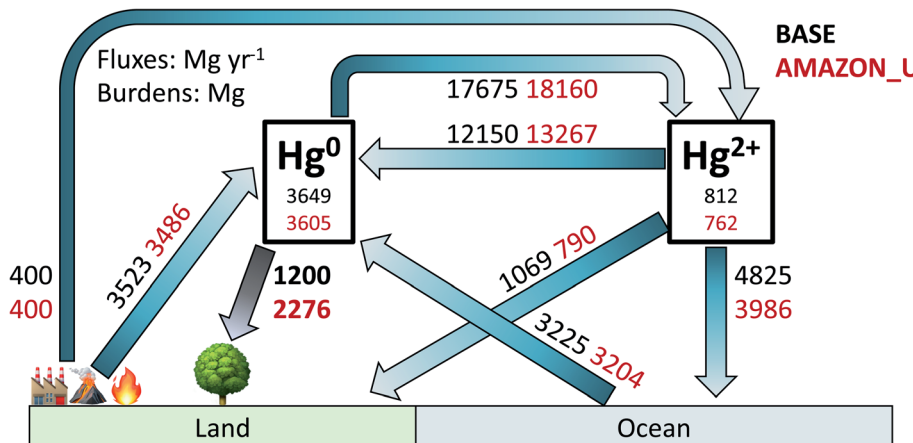


Fig. 6 Atmospheric Hg budget for BASE and AMAZON\_U simulations for year 2015. Atmospheric burdens are listed in units Mg and fluxes in Mg per year. The  $\text{Hg}^{2+}$  burdens and fluxes include both gaseous and particulate  $\text{Hg}^{2+}$ .

considered uptake to moss, lichens, and woody tissues in addition to litterfall.<sup>6</sup> Total Hg deposition to land in AMAZON\_U (2960 Mg per year) also matches with the simulated value from GEM-MACH-Hg (2800 Mg per year).<sup>5</sup> With increased vegetation uptake of  $\text{Hg}^0$ , AMAZON\_U shows improved seasonality of atmospheric  $\text{Hg}^0$  at NH midlatitude sites and reduced biases in  $\text{Hg}^0$  over South America, compared to the BASE simulation. In AMAZON\_U, the increased flux of  $\text{Hg}^0$  dry deposition and reduced fluxes of  $\text{Hg}^{2+}$  deposition (−1118 Mg per year, −19% compared to BASE) helps resolve part of the model bias identified in isotopic  $\Delta^{200}\text{Hg}$  mass balance studies.<sup>29,84</sup> The enhanced role of the land sink in the improved version of GEOS-Chem highlights the importance of considering biosphere-atmosphere feedbacks during climate change in future projections of Hg pollution. Our study also emphasizes the necessity of expanding litterfall monitoring as a lower bound estimate for the magnitude  $\text{Hg}^0$  uptake and conducting additional flux tower studies in different biomes to monitor net ecosystem exchange. Specifically, there are no litterfall flux measurements of Hg from rainforests in Africa or Southeast Asia, which would be invaluable to investigate whether similar uptake processes occur there as in the Amazon.

Our study has improved the  $\text{Hg}^0$  dry deposition parametrization by evaluating GEOS-Chem with a wider array of field evidence (79 studies) than the original parametrization.<sup>51</sup> Nevertheless, the model is still not able to predict observed deposition velocities from individual studies and observed values generally show more variance than modelled values (Fig. 2 and Section S7†). This result indicates that important controls on vegetation uptake could be missing from the GEOS-Chem dry deposition parametrization. For example, the current parametrization<sup>19,20</sup> does not include tree species type or moisture availability, which have been found to influence the variability of foliar Hg uptake across Europe.<sup>10</sup> Other studies highlighted the importance of water availability on plant uptake of ozone, especially when considering the impacts of future climate change, and their expanded parametrizations may serve as examples for future GEOS-Chem development.<sup>65,85</sup> GEOS-

Chem does not explicitly treat the re-emission of  $\text{Hg}^0$  from foliage, which isotopic evidence suggests is around 30% of the gross uptake flux.<sup>86</sup> Other studies have developed bi-directional models of  $\text{Hg}^0$  exchange in the canopy;<sup>40,87</sup> however, the modelled seasonality of  $\text{Hg}^0$  re-emissions<sup>88</sup> disagrees with recent net ecosystem exchange measurements from Harvard Forest.<sup>26</sup> Further combined analysis of field measurements and model parametrizations is essential to implement improved atmosphere-biosphere exchange schemes in chemistry transport models.<sup>15,89</sup>

## 5. Conclusion

Dry deposition of  $\text{Hg}^0$  is a major removal pathway of atmospheric Hg and controls the influx of Hg to terrestrial ecosystems. We conducted model simulations in GEOS-Chem that correspond to different observational constraints of  $\text{Hg}^0$  vegetation uptake. The original BASE simulation agrees with litterfall and total foliar uptake data from outside of the Amazon, yet it cannot capture the seasonality of atmospheric  $\text{Hg}^0$  in the NH midlatitudes and it overestimates atmospheric  $\text{Hg}^0$  in South America. We suggest a higher biological reactivity of  $\text{Hg}^0$  ( $f_0$ ) than the BASE simulation: 0.2 within the Amazon rainforest, in line with available Amazon litterfall and throughfall data,<sup>31</sup> and  $3 \times 10^{-5}$  elsewhere, in line with the existing flux tower study.<sup>26</sup> This simulation (AMAZON\_U) better matches the seasonality of NH midlatitudes  $\text{Hg}^0$  and agrees best with available atmospheric  $\text{Hg}^0$  observations in South America. The revised simulation leads to a global  $\text{Hg}^0$  land sink (2276 Mg per year) that is almost double the original simulation (1200 Mg per year). The Amazon rainforest contributes approximately 29% of the total  $\text{Hg}^0$  land sink worldwide, but continuing deforestation endangers this sink. In the extreme scenario where the entire rainforest is converted to savannah, an additional 283 Mg per year Hg is transferred to the ocean where it can bioaccumulate in the marine food chain. The improved version of GEOS-Chem can be applied in future studies to understand Hg cycle feedbacks between the terrestrial biosphere and the atmosphere.

## Conflicts of interest

There are no conflicts to declare.

## Acknowledgements

This research was funded by an Early Postdoc.Mobility grant (P2EZP2\_195424) from the Swiss National Science Foundation and a grant (#1924148) from the US National Science Foundation. M. J. acknowledges funding from the Swiss National Science Foundation grant PZ00P2\_174101. We thank Daniel Obrist, Katrina MacSween, and Benjamin Geyman for useful discussions during the study preparation. We thank Frits Steenhuisen and Simon Wilson for providing AMAP/UNEP gridded anthropogenic Hg emissions for 2015. We thank Hélène Angot for provision of the Hg measurement data, processing of emission data, and assistance with GEOS-Chem simulations. We thank Frank Wania and Isabel Quant for providing atmospheric Hg<sup>0</sup> data from the LAPAN passive sampler network in South America. We acknowledge the researchers involved in measuring and publishing atmospheric mercury measurements as part of the CAPMoN, EMEP, MDN, AMNet, and GMOS networks. We acknowledge researchers involved in collection of the litterfall, throughfall, and wet deposition measurements included in our compilation dataset.

## References

- 1 UNEP, *Global Mercury Assessment 2018*, UN Environment Programme, Chemicals and Health Branch Geneva, Switzerland, 2019.
- 2 H. M. Horowitz, D. J. Jacob, Y. Zhang, T. S. Dibble, F. Slemr, H. M. Amos, J. A. Schmidt, E. S. Corbett, E. A. Marais and E. M. Sunderland, A new mechanism for atmospheric mercury redox chemistry: implications for the global mercury budget, *Atmos. Chem. Phys.*, 2017, **17**, 6353–6371.
- 3 V. Shah, D. J. Jacob, C. P. Thackray, X. Wang, E. M. Sunderland, T. S. Dibble, A. Saiz-Lopez, I. Černušák, V. Kellö, P. J. Castro, R. Wu and C. Wang, Improved Mechanistic Model of the Atmospheric Redox Chemistry of Mercury, *Environ. Sci. Technol.*, 2021, **55**, 14445–14456.
- 4 M. Jiskra, J. E. Sonke, D. Obrist, J. Bieser, R. Ebinghaus, C. L. Myhre, K. A. Pfaffhuber, I. Wängberg, K. Kyllonen, D. Worthy, L. G. Martin, C. Labuschagne, T. Mkololo, M. Ramonet, O. Magand and A. Dommergue, A vegetation control on seasonal variations in global atmospheric mercury concentrations, *Nat. Geosci.*, 2018, **11**, 244–250.
- 5 J. Zhou, D. Obrist, A. Dastoor, M. Jiskra and A. Ryjkov, Vegetation uptake of mercury and impacts on global cycling, *Nat. Rev. Earth Environ.*, 2021, **2**, 269–284.
- 6 J. Zhou and D. Obrist, Global Mercury Assimilation by Vegetation, *Environ. Sci. Technol.*, 2021, **55**, 14245–14257.
- 7 A. Carpi, A. H. Fostier, O. R. Orta, J. C. dos Santos and M. Gittings, Gaseous mercury emissions from soil following forest loss and land use changes: Field experiments in the United States and Brazil, *Atmos. Environ.*, 2014, **96**, 423–429.
- 8 O. Hararuk, D. Obrist and Y. Luo, Modelling the sensitivity of soil mercury storage to climate-induced changes in soil carbon pools, *Biogeosciences*, 2013, **10**, 2393–2407.
- 9 H. Zhang, C. D. Holmes and S. Wu, Impacts of changes in climate, land use and land cover on atmospheric mercury, *Atmos. Environ.*, 2016, **141**, 230–244.
- 10 L. Wohlgemuth, P. Rautio, B. Ahrends, A. Russ, L. Vesterdal, P. Waldner, V. Timmermann, N. Eickenscheidt, A. Fürst, M. Greve, P. Roskams, A. Thimonier, M. Nicolas, A. Kowalska, M. Ingerslev, P. Merilä, S. Benham, C. Iacoban, G. Hoch, C. Alewell and M. Jiskra, Physiological and climate controls on foliar mercury uptake by European tree species, *Biogeosciences*, 2022, **19**, 1335–1353.
- 11 Y. Yang, L. Meng, R. D. Yanai, M. Montesdeoca, P. H. Templer, H. Asbjørnsen, L. E. Rustad and C. T. Driscoll, Climate change may alter mercury fluxes in northern hardwood forests, *Biogeochemistry*, 2019, **146**, 1–16.
- 12 I. Amigo, When will the Amazon hit a tipping point?, *Nature*, 2020, **578**, 505–508.
- 13 O. Hoegh-Guldberg, D. Jacob, M. Taylor, M. Bindi, S. Brown, I. Camilloni, A. Diedhiou, R. Djalante, K. Ebi, F. Engelbrecht, J. Guiot, Y. Hijioka, S. Mehrotra, A. Payne, S. I. Seneviratne, A. Thomas, R. Warren and G. Zhou, in *Global Warming of 1.5°C. An IPCC Special Report on the Impacts of Global Warming of 1.5°C above Pre-industrial Levels and Related Global Greenhouse Gas Emission Pathways, in the Context of Strengthening the Global Response to the Threat of Climate Change*, ed. V. Masson-Delmotte, P. Zhai, H. O. Pörtner, D. Roberts, J. Skea, P. R. Shukla, A. Pirani, W. Moufouma-Okia, C. Péan, R. Pidcock, S. Connors, J. B. R. Matthews, Y. Chen, X. Zhou, M. I. Gomis, E. Lonnoy, T. Maycock, M. Tignor and T. Waterfield, World Meteorological Organization Technical Document, 2018.
- 14 C. A. Nobre, G. Sampaio, L. S. Borma, J. C. Castilla-Rubio, J. S. Silva and M. Cardoso, Land-use and climate change risks in the Amazon and the need of a novel sustainable development paradigm, *Proc. Natl. Acad. Sci. U. S. A.*, 2016, **113**, 10759–10768.
- 15 T. R. Khan, D. Obrist, Y. Agnan, N. E. Selin and J. A. Perlinder, Atmosphere-terrestrial exchange of gaseous elemental mercury: parameterization improvement through direct comparison with measured ecosystem fluxes, *Environ. Sci.: Processes Impacts*, 2019, **21**, 1699–1712.
- 16 S. Song, N. E. Selin, A. L. Soerensen, H. Angot, R. Artz, S. Brooks, E.-G. Brunke, G. Conley, A. Dommergue, R. Ebinghaus, T. M. Holsen, D. A. Jaffe, S. Kang, P. Kelley, W. T. Luke, O. Magand, K. Marumoto, K. A. Pfaffhuber, X. Ren, G.-R. Sheu, F. Slemr, T. Warneke, A. Weigelt, P. Weiss-Penzias, D. C. Wip and Q. Zhang, Top-down constraints on atmospheric mercury emissions and implications for global biogeochemical cycling, *Atmos. Chem. Phys.*, 2015, **15**, 7103–7125.
- 17 V. L. St. Louis, J. A. Graydon, I. Lehnher, H. M. Amos, E. M. Sunderland, K. A. St. Pierre, C. A. Emmerton, K. Sandilands, M. Tate, A. Steffen and E. R. Humphreys, Atmospheric Concentrations and Wet/Dry Loadings of



Mercury at the Remote Experimental Lakes Area, Northwestern Ontario, Canada, *Environ. Sci. Technol.*, 2019, **53**, 8017–8026.

18 O. Travnikov, H. Angot, P. Artaxo, M. Bencardino, J. Bieser, F. D'Amore, A. Dastoor, F. De Simone, M. del C. Diéguez, A. Dommergues, R. Ebinghaus, X. B. Feng, C. N. Gencarelli, I. M. Hedgecock, O. Magand, L. Martin, V. Matthias, N. Mashyanov, N. Pirrone, R. Ramachandran, K. A. Read, A. Ryjkov, N. E. Selin, F. Sena, S. Song, F. Sprovieri, D. Wip, I. Wängberg and X. Yang, Multi-model study of mercury dispersion in the atmosphere: atmospheric processes and model evaluation, *Atmos. Chem. Phys.*, 2017, **17**, 5271–5295.

19 Y. Wang, D. J. Jacob and J. A. Logan, Global simulation of tropospheric  $O_3$ -NO $_x$ -hydrocarbon chemistry: 1. Model formulation, *J. Geophys. Res.*, 1998, **103**, 10713–10725.

20 M. L. Wesely, Parameterization of surface resistances to gaseous dry deposition in regional-scale numerical models, *Atmos. Environ.*, 1989, **23**, 1293–1304.

21 J. D. Demers, J. D. Blum and D. R. Zak, Mercury isotopes in a forested ecosystem: Implications for air-surface exchange dynamics and the global mercury cycle, *Global Biogeochem. Cycles*, 2013, **27**, 222–238.

22 M. Jiskra, J. G. Wiederhold, U. Skyllberg, R.-M. Kronberg, I. Hajdas and R. Kretzschmar, Mercury Deposition and Re-emission Pathways in Boreal Forest Soils Investigated with Hg Isotope Signatures, *Environ. Sci. Technol.*, 2015, **49**, 7188–7196.

23 W. Zheng, D. Obrist, D. Weis and B. A. Bergquist, Mercury isotope compositions across North American forests: Mercury Isotopes Across U.S. Forests, *Global Biogeochem. Cycles*, 2016, **30**, 1475–1492.

24 L. P. Wright, L. Zhang and F. J. Marsik, Overview of mercury dry deposition, litterfall, and throughfall studies, *Atmos. Chem. Phys.*, 2016, **16**, 13399–13416.

25 X. Wang, W. Yuan, C.-J. Lin, J. Luo, F. Wang, X. Feng, X. Fu and C. Liu, Underestimated Sink of Atmospheric Mercury in a Deglaciated Forest Chronosequence, *Environ. Sci. Technol.*, 2020, **54**, 8083–8093.

26 D. Obrist, E. M. Roy, J. L. Harrison, C. F. Kwong, J. W. Munger, H. Moosmüller, C. D. Romero, S. Sun, J. Zhou and R. Commane, Previously unaccounted atmospheric mercury deposition in a midlatitude deciduous forest, *Proc. Natl. Acad. Sci. U. S. A.*, 2021, **118**, e2105477118.

27 X. Wang, Z. Bao, C.-J. Lin, W. Yuan and X. Feng, Assessment of Global Mercury Deposition through Litterfall, *Environ. Sci. Technol.*, 2016, **50**, 8548–8557.

28 X. Fu, W. Zhu, H. Zhang, J. Sommar, B. Yu, X. Yang, X. Wang, C.-J. Lin and X. Feng, Depletion of atmospheric gaseous elemental mercury by plant uptake at Mt. Changbai, Northeast China, *Atmos. Chem. Phys.*, 2016, **16**, 12861–12873.

29 X. Fu, M. Jiskra, X. Yang, N. Maruszczak, M. Enrico, J. Chmeleff, L.-E. Heimbürger-Boavida, F. Gheusi and J. E. Sonke, Mass-Independent Fractionation of Even and Odd Mercury Isotopes during Atmospheric Mercury Redox Reactions, *Environ. Sci. Technol.*, 2021, **55**, 10164–10174.

30 D. Obrist, J. L. Kirk, L. Zhang, E. M. Sunderland, M. Jiskra and N. E. Selin, A review of global environmental mercury processes in response to human and natural perturbations: Changes of emissions, climate, and land use, *Ambio*, 2018, **47**, 116–140.

31 A. H. Fostier, J. J. Melendez-Perez and L. Richter, Litter mercury deposition in the Amazonian rainforest, *Environ. Pollut.*, 2015, **206**, 605–610.

32 J. Zhou, B. Du, L. Shang, Z. Wang, H. Cui, X. Fan and J. Zhou, Mercury fluxes, budgets, and pools in forest ecosystems of China: A review, *Crit. Rev. Environ. Sci. Technol.*, 2020, **50**, 1411–1450.

33 Y. Zhang, D. J. Jacob, H. M. Horowitz, L. Chen, H. M. Amos, D. P. Krabbenhoft, F. Slemr, V. L. St. Louis and E. M. Sunderland, Observed decrease in atmospheric mercury explained by global decline in anthropogenic emissions, *Proc. Natl. Acad. Sci. U. S. A.*, 2016, **113**, 526–531.

34 D. A. Gay, D. Schmeltz, E. Prestbo, M. Olson, T. Sharac and R. Tordon, The Atmospheric Mercury Network: measurement and initial examination of an ongoing atmospheric mercury record across North America, *Atmos. Chem. Phys.*, 2013, **13**, 11339–11349.

35 A. Cole, A. Steffen, C. Eckley, J. Narayan, M. Pilote, R. Tordon, J. Graydon, V. St. Louis, X. Xu and B. Branfireun, A Survey of Mercury in Air and Precipitation across Canada: Patterns and Trends, *Atmosphere*, 2014, **5**, 635–668.

36 K. Tørseth, W. Aas, K. Breivik, A. M. Fjæraa, M. Fiebig, A. G. Hjelbrekke, C. Lund Myhre, S. Solberg and K. E. Yttri, Introduction to the European Monitoring and Evaluation Programme (EMEP) and observed atmospheric composition change during 1972–2009, *Atmos. Chem. Phys.*, 2012, **12**, 5447–5481.

37 F. Sprovieri, N. Pirrone, M. Bencardino, F. D'Amore, F. Carbone, S. Cinnirella, V. Mannarino, M. Landis, R. Ebinghaus, A. Weigelt, E.-G. Brunke, C. Labuschagne, L. Martin, J. Munthe, I. Wängberg, P. Artaxo, F. Morais, H. de M. J. Barbosa, J. Brito, W. Cairns, C. Barbante, M. del C. Diéguez, P. E. Garcia, A. Dommergues, H. Angot, O. Magand, H. Skov, M. Horvat, J. Kotnik, K. A. Read, L. M. Neves, B. M. Gawlik, F. Sena, N. Mashyanov, V. Obolkin, D. Wip, X. B. Feng, H. Zhang, X. Fu, R. Ramachandran, D. Cossa, J. Knoery, N. Maruszczak, M. Nerentorp and C. Norstrom, Atmospheric mercury concentrations observed at ground-based monitoring sites globally distributed in the framework of the GMOS network, *Atmos. Chem. Phys.*, 2016, **16**, 11915–11935.

38 R. Gelaro, W. McCarty, M. J. Suárez, R. Todling, A. Molod, L. Takacs, C. A. Randles, A. Darmenov, M. G. Bosilovich, R. Reichle, K. Wargan, L. Coy, R. Cullather, C. Draper, S. Akella, V. Buchard, A. Conaty, A. M. da Silva, W. Gu, G.-K. Kim, R. Koster, R. Lucchesi, D. Merkova, J. E. Nielsen, G. Partyka, S. Pawson, W. Putman, M. Riener, S. D. Schubert, M. Sienkiewicz and B. Zhao, The Modern-Era Retrospective Analysis for Research and Applications, Version 2 (MERRA-2), *J. Clim.*, 2017, **30**, 5419–5454.



39 D. Obrist, W. Munger and R. Commane, *Atmospheric Gaseous Elemental Mercury Fluxes at Harvard Forest EMS Tower 2019–2020 Ver 1*, 2021, DOI: DOI: [10.6073/pasta/0d9d994b069bc1d2a11eb9a7dc783bff](https://doi.org/10.6073/pasta/0d9d994b069bc1d2a11eb9a7dc783bff).

40 L. P. Wright and L. Zhang, An approach estimating bidirectional air-surface exchange for gaseous elemental mercury at AMNet sites, *J. Adv. Model. Earth Syst.*, 2015, **7**, 35–49.

41 J. A. Schmidt, D. J. Jacob, H. M. Horowitz, L. Hu, T. Sherwen, M. J. Evans, Q. Liang, R. M. Suleiman, D. E. Oram, M. Le Breton, C. J. Percival, S. Wang, B. Dix and R. Volkamer, Modeling the observed tropospheric BrO background: Importance of multiphase chemistry and implications for ozone, OH, and mercury, *J. Geophys. Res.: Atmos.*, 2016, **121**, 11819–11835.

42 T. S. Dibble, H. L. Tetu, Y. Jiao, C. P. Thackray and D. J. Jacob, Modeling the OH-Initiated Oxidation of Mercury in the Global Atmosphere without Violating Physical Laws, *J. Phys. Chem. A*, 2020, **124**, 444–453.

43 A. Saiz-Lopez, O. Travnikov, J. E. Sonke, C. P. Thackray, D. J. Jacob, J. Carmona-García, A. Francés-Monerris, D. Roca-Sanjuán, A. U. Acuña, J. Z. Dávalos, C. A. Cuevas, M. Jiskra, F. Wang, J. Bieser, J. M. C. Plane and J. S. Francisco, Photochemistry of oxidized Hg(I) and Hg(II) species suggests missing mercury oxidation in the troposphere, *Proc. Natl. Acad. Sci. U. S. A.*, 2020, **117**, 30949–30956.

44 X. Wang, D. J. Jacob, W. Downs, S. Zhai, L. Zhu, V. Shah, C. D. Holmes, T. Sherwen, B. Alexander, M. J. Evans, S. D. Eastham, J. A. Neuman, P. R. Veres, T. K. Koenig, R. Volkamer, L. G. Huey, T. J. Bannan, C. J. Percival, B. H. Lee and J. A. Thornton, Global tropospheric halogen (Cl, Br, I) chemistry and its impact on oxidants, *Atmos. Chem. Phys.*, 2021, **21**, 13973–13996.

45 H. M. Amos, D. J. Jacob, C. D. Holmes, J. A. Fisher, Q. Wang, R. M. Yantosca, E. S. Corbitt, E. Galarneau, A. P. Rutter, M. S. Gustin, A. Steffen, J. J. Schauer, J. A. Graydon, V. L. St. Louis, R. W. Talbot, E. S. Edgerton, Y. Zhang and E. M. Sunderland, Gas-particle partitioning of atmospheric Hg(II) and its effect on global mercury deposition, *Atmos. Chem. Phys.*, 2012, **12**, 591–603.

46 H. Liu, D. J. Jacob, I. Bey and R. M. Yantosca, Constraints from 210 Pb and 7 Be on wet deposition and transport in a global three-dimensional chemical tracer model driven by assimilated meteorological fields, *J. Geophys. Res.*, 2001, **106**, 12109–12128.

47 D. J. Jacob and S. C. Wofsy, Budgets of reactive nitrogen, hydrocarbons, and ozone over the Amazon forest during the wet season, *J. Geophys. Res.*, 1990, **95**, 16737.

48 H. K. Gibbs, *Olson's Major World Ecosystem Complexes Ranked by Carbon in Live Vegetation: an Updated Database Using the GLC2000 Land Cover Product (NDP-017b)*, 2006, <https://www.osti.gov/biblio/1389498>.

49 H. Yuan, Y. Dai, Z. Xiao, D. Ji and W. Shangguan, Reprocessing the MODIS Leaf Area Index products for land surface and climate modelling, *Remote Sens. Environ.*, 2011, **115**, 1171–1187.

50 C.-J. Lin and S. O. Pehkonen, The chemistry of atmospheric mercury: a review, *Atmos. Environ.*, 1999, **33**, 2067–2079.

51 N. E. Selin, D. J. Jacob, R. M. Yantosca, S. Strode, L. Jaeglé and E. M. Sunderland, Global 3-D land-ocean-atmosphere model for mercury: Present-day versus preindustrial cycles and anthropogenic enrichment factors for deposition, *Global Biogeochem. Cycles*, 2008, **22**, GB2011.

52 S. A. Strode, L. Jaeglé, N. E. Selin, D. J. Jacob, R. J. Park, R. M. Yantosca, R. P. Mason and F. Slemr, Air-sea exchange in the global mercury cycle, *Global Biogeochem. Cycles*, 2007, **21**, GB1017.

53 J. A. Fisher, D. J. Jacob, Q. Wang, R. Bahreini, C. C. Carouge, M. J. Cubison, J. E. Dibb, T. Diehl, J. L. Jimenez, E. M. Leibensperger, Z. Lu, M. B. J. Meinders, H. O. T. Pye, P. K. Quinn, S. Sharma, D. G. Streets, A. van Donkelaar and R. M. Yantosca, Sources, distribution, and acidity of sulfate–ammonium aerosol in the Arctic in winter–spring, *Atmos. Environ.*, 2011, **45**, 7301–7318.

54 L. Zhang, S. Gong, J. Padro and L. Barrie, A size-segregated particle dry deposition scheme for an atmospheric aerosol module, *Atmos. Environ.*, 2001, **35**, 549–560.

55 F. Steenhuisen and S. J. Wilson, *Geospatially Distributed (Gridded) Global Mercury Emissions to Air from Anthropogenic Sources in 2015*, 2022, DOI: DOI: [10.34894/SZ2KOI](https://doi.org/10.34894/SZ2KOI).

56 F. Steenhuisen and S. J. Wilson, Development and application of an updated geospatial distribution model for gridding 2015 global mercury emissions, *Atmos. Environ.*, 2019, **211**, 138–150.

57 Y. Zhang, D. J. Jacob, S. Dutkiewicz, H. M. Amos, M. S. Long and E. M. Sunderland, Biogeochemical drivers of the fate of riverine mercury discharged to the global and Arctic oceans, *Global Biogeochem. Cycles*, 2015, **29**, 854–864.

58 L. Zhang, L. P. Wright and P. Blanchard, A review of current knowledge concerning dry deposition of atmospheric mercury, *Atmos. Environ.*, 2009, **43**, 5853–5864.

59 L. Zhang, P. Blanchard, D. A. Gay, E. M. Prestbo, M. R. Risch, D. Johnson, J. Narayan, R. Zsolway, T. M. Holsen, E. K. Miller, M. S. Castro, J. A. Graydon, V. L. St. Louis and J. Dalziel, Estimation of speciated and total mercury dry deposition at monitoring locations in eastern and central North America, *Atmos. Chem. Phys.*, 2012, **12**, 4327–4340.

60 S. J. Silva and C. L. Heald, Investigating Dry Deposition of Ozone to Vegetation, *J. Geophys. Res.: Atmos.*, 2018, **123**, 559–573.

61 G. J. McRae, W. R. Goodin and J. H. Seinfeld, Development of a second-generation mathematical model for Urban air pollution—I. Model formulation, *Atmos. Environ.*, 1982, **16**, 679–696.

62 B. F. Alves de Oliveira, M. J. Bottino, P. Nobre and C. A. Nobre, Deforestation and climate change are projected to increase heat stress risk in the Brazilian Amazon, *Commun. Earth Environ.*, 2021, **2**, 207.

63 J. R. P. Peleja, *Balanço de massas de mercúrio (Hg) total em duas microbacias da Amazônia Central*, Instituto Nacional de Pesquisas da Amazônia-INPA, <https://repositorio.inpa.gov.br/handle/1/11464>, 2007.



64 J. R. Gerson, N. Szponar, A. A. Zambrano, B. Bergquist, E. Broadbent, C. T. Driscoll, G. Erkenswick, D. C. Evers, L. E. Fernandez, H. Hsu-Kim, G. Inga, K. N. Lansdale, M. J. Marchese, A. Martinez, C. Moore, W. K. Pan, R. P. Purizaca, V. Sánchez, M. Silman, E. A. Ury, C. Vega, M. Watsa and E. S. Bernhardt, Amazon forests capture high levels of atmospheric mercury pollution from artisanal gold mining, *Nat. Commun.*, 2022, **13**, 559.

65 M. Lin, S. Malyshev, E. Shevlakova, F. Paulot, L. W. Horowitz, S. Fares, T. N. Mikkelsen and L. Zhang, Sensitivity of Ozone Dry Deposition to Ecosystem-Atmosphere Interactions: A Critical Appraisal of Observations and Simulations, *Global Biogeochem. Cycles*, 2019, **33**, 1264–1288.

66 C. D. Holmes, D. J. Jacob, E. S. Corbitt, J. Mao, X. Yang, R. Talbot and F. Slemr, Global atmospheric model for mercury including oxidation by bromine atoms, *Atmos. Chem. Phys.*, 2010, **10**, 12037–12057.

67 A. M. Koenig, O. Magand, P. Laj, M. Andrade, I. Moreno, F. Velarde, G. Salvatierra, R. Gutierrez, L. Blacutt, D. Aliaga, T. Reichler, K. Sellegrí, O. Laurent, M. Ramonet and A. Dommergue, Seasonal patterns of atmospheric mercury in tropical South America as inferred by a continuous total gaseous mercury record at Chacaltaya station (5240 m) in Bolivia, *Atmos. Chem. Phys.*, 2021, **21**, 3447–3472.

68 M. I. Quant, MSc thesis, University of Toronto, 2021, <http://hdl.handle.net/1807/109628>.

69 C. D. Holmes, N. P. Krishnamurthy, J. M. Caffrey, W. M. Landing, E. S. Edgerton, K. R. Knapp and U. S. Nair, Thunderstorms Increase Mercury Wet Deposition, *Environ. Sci. Technol.*, 2016, **50**, 9343–9350.

70 X. Xu, X. Feng, H. Lin, P. Zhang, S. Huang, Z. Song, Y. Peng, T.-M. Fu and Y. Zhang, Modelling the High Mercury Wet deposition in the Southeastern US by WRF-GC, *Geosci. Model Dev. Discuss.*, 2022, 1–21.

71 Y. Zhang, L. Jaeglé, A. van Donkelaar, R. V. Martin, C. D. Holmes, H. M. Amos, Q. Wang, R. Talbot, R. Artz, S. Brooks, W. Luke, T. M. Holsen, D. Felton, E. K. Miller, K. D. Perry, D. Schmeltz, A. Steffen, R. Tordon, P. Weiss-Penzias and R. Zsolnay, Nested-grid simulation of mercury over North America, *Atmos. Chem. Phys.*, 2012, **12**, 6095–6111.

72 K. Liu, Q. Wu, L. Wang, S. Wang, T. Liu, D. Ding, Y. Tang, G. Li, H. Tian, L. Duan, X. Wang, X. Fu, X. Feng and J. Hao, Measure-Specific Effectiveness of Air Pollution Control on China's Atmospheric Mercury Concentration and Deposition during 2013–2017, *Environ. Sci. Technol.*, 2019, **53**, 8938–8946.

73 I. Cheng, L. Zhang and H. Mao, Relative contributions of gaseous oxidized mercury and fine and coarse particle-bound mercury to mercury wet deposition at nine monitoring sites in North America, *J. Geophys. Res.: Atmos.*, 2015, **120**, 8549–8562.

74 L. V. Gatti, L. S. Basso, J. B. Miller, M. Gloor, L. Gatti Domingues, H. L. G. Cassol, G. Tejada, L. E. O. C. Aragão, C. Nobre, W. Peters, L. Marani, E. Arai, A. H. Sanches, S. M. Corrêa, L. Anderson, C. Von Randow, C. S. C. Correia, S. P. Crispim and R. A. L. Neves, Amazonia as a carbon source linked to deforestation and climate change, *Nature*, 2021, **595**, 388–393.

75 T. E. Lovejoy and C. Nobre, Amazon Tipping Point, *Sci. Adv.*, 2018, **4**, eaat2340.

76 G. P. Asner, W. Llactayo, R. Tupayachi and E. R. Luna, Elevated rates of gold mining in the Amazon revealed through high-resolution monitoring, *Proc. Natl. Acad. Sci. U. S. A.*, 2013, **110**, 18454–18459.

77 F. Lobo, M. Costa, E. Novo and K. Telmer, Distribution of Artisanal and Small-Scale Gold Mining in the Tapajós River Basin (Brazilian Amazon) over the Past 40 Years and Relationship with Water Siltation, *Remote Sens.*, 2016, **8**, 579.

78 H. Selin, S. E. Keane, S. Wang, N. E. Selin, K. Davis and D. Bally, Linking science and policy to support the implementation of the Minamata Convention on Mercury, *Ambio*, 2018, **47**, 198–215.

79 S. E. Diringer, A. J. Berk, M. Marani, E. J. Ortiz, O. Karatum, D. L. Plata, W. K. Pan and H. Hsu-Kim, Deforestation Due to Artisanal and Small-Scale Gold Mining Exacerbates Soil and Mercury Mobilization in Madre de Dios, Peru, *Environ. Sci. Technol.*, 2020, **54**, 286–296.

80 P. A. M. Michelazzo, A. H. Fostier, G. Magarelli, J. C. Santos and J. A. de Carvalho, Mercury emissions from forest burning in southern Amazon, *Geophys. Res. Lett.*, 2010, **37**, L09809.

81 L. F. F. G. Assis, K. R. Ferreira, L. Vinhas, L. Maurano, C. Almeida, A. Carvalho, J. Rodrigues, A. Maciel and C. Camargo, TerraBrasilis: A Spatial Data Analytics Infrastructure for Large-Scale Thematic Mapping, *ISPRS Int. J. Geo-Inf.*, 2019, **8**, 513.

82 H. M. Amos, D. J. Jacob, D. G. Streets and E. M. Sunderland, Legacy impacts of all-time anthropogenic emissions on the global mercury cycle, *Global Biogeochem. Cycles*, 2013, **27**, 410–421.

83 J. R. Gerson, S. N. Topp, C. M. Vega, J. R. Gardner, X. Yang, L. E. Fernandez, E. S. Bernhardt and T. M. Pavelsky, Artificial lake expansion amplifies mercury pollution from gold mining, *Sci. Adv.*, 2020, **6**, eabd4953.

84 M. Jiskra, L.-E. Heimbürger-Boavida, M.-M. Desgranges, M. V. Petrova, A. Dufour, B. Ferreira-Araujo, J. Masbou, J. Chmeleff, M. Thyssen, D. Point and J. E. Sonke, Mercury stable isotopes constrain atmospheric sources to the ocean, *Nature*, 2021, **597**, 678–682.

85 O. E. Clifton, D. L. Lombardozzi, A. M. Fiore, F. Paulot and L. W. Horowitz, Stomatal conductance influences interannual variability and long-term changes in regional cumulative plant uptake of ozone, *Environ. Res. Lett.*, 2020, **15**, 114059.

86 W. Yuan, J. Sommar, C.-J. Lin, X. Wang, K. Li, Y. Liu, H. Zhang, Z. Lu, C. Wu and X. Feng, Stable Isotope Evidence Shows Re-emission of Elemental Mercury Vapor Occurring after Reductive Loss from Foliage, *Environ. Sci. Technol.*, 2019, **53**, 651–660.

87 J. O. Bash, Description and initial simulation of a dynamic bidirectional air-surface exchange model for mercury in



Community Multiscale Air Quality (CMAQ) model, *J. Geophys. Res.*, 2010, **115**, D06305.

88 L. Zhang, Z. Wu, I. Cheng, L. P. Wright, M. L. Olson, D. A. Gay, M. R. Risch, S. Brooks, M. S. Castro, G. D. Conley, E. S. Edgerton, T. M. Holsen, W. Luke, R. Tordon and P. Weiss-Penzias, The Estimated Six-Year Mercury Dry Deposition Across North America, *Environ. Sci. Technol.*, 2016, **50**, 12864–12873.

89 E. W. Emerson, A. L. Hodshire, H. M. DeBolt, K. R. Bilsback, J. R. Pierce, G. R. McMeeking and D. K. Farmer, Revisiting particle dry deposition and its role in radiative effect estimates, *Proc. Natl. Acad. Sci. U. S. A.*, 2020, **117**, 26076–26082.

90 A. H. Fostier, M. C. Forti, J. R. Guimarães, A. J. Melfi, R. Boulet, C. M. Espírito Santo and F. J. Krug, Mercury fluxes in a natural forested Amazonian catchment (Serra do Navio, Amapá State, Brazil), *Sci. Total Environ.*, 2000, **260**, 201–211.

91 AMAP/UN Environment, *Technical Background Report for the Global Mercury Assessment 2018, Arctic Monitoring and Assessment Programme*, Oslo, Norway/UN Environment Programme, Chemicals and Health Branch, Geneva, Switzerland, 2019.

